Minimum-time manoeuvring in electric vehicles with four wheel-individual-motors

Ricardo de Castro[a], Mara Tanelli[b*], Rui Esteves Araújo[c] and Sergio M. Savaresi[b]

[a]Institute of System Dynamics and Control, Robotics and Mechatronics Center, German Aerospace Center (DLR), Wessling, D-82234, Germany; [b]Dipartimento di Elettronica, Informazione e Bioingegneria, Politecnico di Milano, Piazza Leonardo da Vinci 32, 20133 Milano, Italy; [c]INESC TEC (formerly INESC Porto) and Faculty of Engineering, University of Porto, Rua Dr. Roberto Frias, s/n 4200-465 Porto, Portugal

1. Introduction and motivation

Torque allocation for over-actuated vehicles is a very interesting and challenging research topic in Automotive systems. The most modern vehicle architectures, in fact, offer a plurality of actuators that allow actively shaping the vehicle dynamic response. This active shaping can be performed by properly setting up hierarchical control problems that regulate the vehicle motion by allocating the torques at the wheels and then solving constrained control allocation problems that optimise different cost functions, that can be either safety, or energy, or performance oriented (or, most interestingly, combinations of all these aspects), see e.g. [1]. Usually, the high-level motion objectives are expressed in terms of imposing a desired yaw-moment to the vehicle, which must then be transformed in wheel torque reference signals (or torque differences).

For power trains endowed with wheel individual motors (WIMs), which can be either in-wheel motors or close to the wheel, the emulation of the open mechanical differential is, perhaps, the simplest strategy that can be used for the torque allocation problem, which leads to apply the same torque to the left and right wheels, see e.g. [2]. While this strategy may

---

*Corresponding author. Email:
tanelli@elet.polimi.it

c

improve the driving experience in off-road conditions, it is obvious that it cannot take full advantage of the torque- capabilities offered by the WIMs. Along the same lines, the concept of electric differential (see [3–6]) has recently been developed: the main idea is to make the speed of the inside/outside wheels (or, alternatively, the speed difference) follows a set-point generated by a kinematic model, based on the Ackermann steering geometry. While it may be useful in low-speed manoeuvres, the fact that kinematic models do not take into account the lateral dynamics makes this approach unsuitable to improve the vehicle- properties or its safety when driving close to the friction limits.

From the vehicle dynamics viewpoint, the application of different forces on the left/right wheels produces an additional yaw-moment, which can be seen as a valuable control input to actively modify the vehicle and ensure a safe motion. In this framework, also known in the literature as the direct yaw-moment control, there are three major issues that must addressed: (i) generation of the yaw-rate reference, (ii) vehicle force control and (iii) wheel torque allocation. The most common approach to generate the yaw-rate set-point is to use as reference the steady-state response of the bicycle model,[7] or, alternatively, employ the understeer curves.[8] In both cases, the desired vehicle- characteristics, such as neutral, understeer or oversteer behaviour, can be straightforwardly specified (e.g. through the well-known *understeer gradient* parameter). In addition to the steady-state behaviour, one may also specify the desired transient response, such as the yaw-rate damping and rising times,[9] which are crucial to actively modify the vehicle responsiveness and agility. Once the yaw reference has been found, it is necessary to design a control law that can impose this reference. There is a wide range of possibilities for designing such a controller, ranging from linear and time-invariant controllers,[10,11] linear quadratic regulator,[12,13] internal model control,[8] sliding mode control,[14,15] model-predictive controller.[16] One of the main challenges in the design of these controllers is to ensure robust operation in the presence of model uncertainties, e.g. in the tyre–road friction coefficient.

Notice that, although some of these studies consider that the additional yaw-moment is generated through differential braking and/or active mechanical differential, from a theoretical point of view the control algorithms can be straightforwardly adapted to power train configurations equipped with WIMs.

Finally, the yaw-moment requested by the controller must be translated into a wheel torque reference. When the actuators are installed in only one axle (e.g. with torque- devices or with 2 WIMs), the allocation is relatively straightforward to perform because there is a one-to-one mapping between the yaw-moment and the force difference in the axle's wheels.[8,12,17] On the other hand, if 4 WIMs are present there is redundancy in the moment generation, which can be explored to minimise the energy consumption [1,15] or the friction use of the tyres,[18,19] through the use of optimisation-based techniques. In both cases, the torque allocation must also take into account the saturation of the power train actuators, such as the limited torque range and torque rates of the WIMs and friction brakes, and handle the friction limits of the tyres, e.g. due to the well-known friction ellipse constraints.[19]

The approaches developed so far are, undoubtedly, very attractive and can ensure a safe and energy-efficient operation of vehicle when the accelerations are moderate (see the gg diagram in Figure 1). However, as the vehicle approaches its operation limits (see 'zone B' in Figure 1), one may question if the existing allocation schemes will be able to extract the maximum performance from the vehicle (e.g. to operate near the friction limits when one has combined steering and acceleration/braking).

In this context, the main contributions of this paper are the following: (i) to investigate torque allocation strategies that allow the driver to extract the maximum performance from the electric vehicle (EV), i.e. minimise the lap-time, without trying to correct the trajectory or stabilise the vehicle motion (which are, instead, the main concerns when operating in zone B
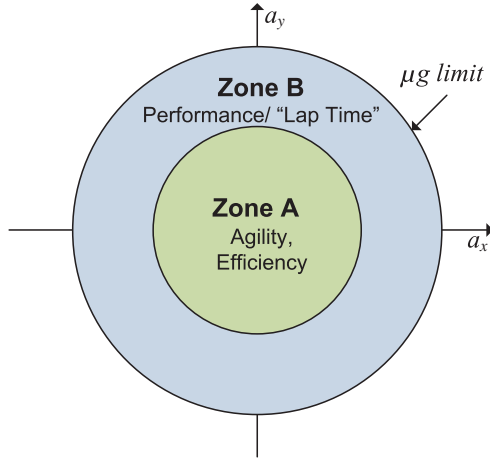
Figure 1. Performance zones in the gg diagram.

of Figure 1). (ii) to extend the preliminary results presented in [20] and formulate an optimal problem that allows determining the torque distribution among the 4 WIMs that makes the EV perform a given manoeuvre in a minimum time, according to the minimum-time manoeuvring problem, see [21], which has emerged in recent years as a key tool for determining the optimal trajectory and driver inputs [22,23] in the racing context. In the present work, this framework will be revisited to devise a benchmark, a-causal torque allocation solution, against which the online strategies can be objectively evaluated. (iii) To propose a causal, online, sub-optimal allocation strategy that uses only the current and past values of the driver's inputs (steer, throttle and brake pedal) and the vehicle state (longitudinal and lateral acceleration), and compare it against the a-causal, offline one to assess the performance of the torque distribution algorithm. Although the torque distribution issue has been previously addressed in the literature, see e.g. [24–26], these studies are essentially focused on the theoretical assessment of the impact of the WIMs on the operational envelope of the vehicle. Furthermore, none of these previous studies investigated in detail how to perform the mapping between the driver inputs/vehicle states and individual wheel torques, which is discussed herein.

To the best of our knowledge, the state of art on 'minimum-time manoeuvring for EVs with 4 WIMs is very limited'. Most of the previous works on the torque allocation for EVs with 4 WIMs focused on improving the vehicle , and on the exploration of the additional yaw-moment needed to stabilise the yaw-rate and/or the vehicle side-slip. In this work, our main motivation is to extend the research view by focusing on strategies that can promote the minimisation of the manoeuvre time in a sport environment.

The remainder of the paper is structured as follows. Section 2 presents the vehicle model adopted in this work, while Section 3 illustrates the optimal control policy that defines the benchmark solution for the allocation problem. Furthermore, Section 4 presents the causal allocation strategy, the performance of which is discussed in Section 5.

2. Vehicle model

In this section, a two-track, nonlinear vehicle model will be introduced, which will serve as a basis for the torque allocation strategies. To make the model tractable, the roll and pitch dynamics of the EV are neglected, as commonly done in this context.[8,27,28]
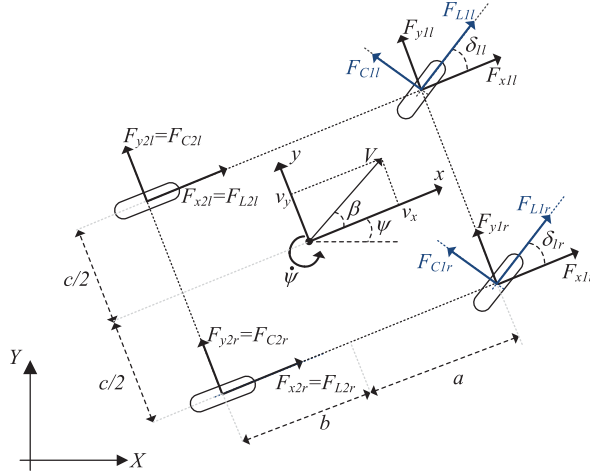
Figure 2. Representation of the vehicle model. Notation: *XY* -axis is fixed with the earth, *xy* with the vehicle's CoG, *LC* with the wheels. The subscript $1j, j \in \{l, r\}$, refers to the vehicle's wheels, while $2j$ refers to the rears.

Consider the vehicle represented in Figure 2, as well as the vector $\mathbf{p} = [X \ Y \ \psi]^{\mathrm{T}}$, which characterises the position and orientation of the vehicle centre of gravity (CoG) in the *XY* -axis system, fixed with earth. The dynamic evolution of $\mathbf{p}$ can be defined as

$$\underbrace{\begin{bmatrix} m & 0 & 0 \\ 0 & m & 0 \\ 0 & 0 & I_z \end{bmatrix}}_{\mathbf{M}} \ddot{\mathbf{p}} = \underbrace{\begin{bmatrix} \cos(\psi) & -\sin(\psi) & 0 \\ \sin(\psi) & \cos(\psi) & 0 \\ 0 & 0 & 1 \end{bmatrix}}_{\mathbf{T}(\mathbf{p})} \left(\begin{bmatrix} F_x \\ F_y \\ M_z \end{bmatrix} - \Delta \right),$$

where m is the vehicle mass, I_z the yaw inertia, $\Delta \in \mathbb{R}^3$ a vector of disturbances, defined in Appendix 2, (F_x, F_y) are the generalised forces, applied to the vehicle CoG and M_z the generalised yaw-moment; the matrix $\mathbf{T}(\mathbf{p})$ represents a change of coordinates between the *xy* frame (integral to the CoG) and the XY coordinates. The equations of vehicle motion can also be compactly represented as

$$\mathbf{M}\ddot{\mathbf{p}} = \mathbf{T}(\mathbf{p})(\mathcal{F} - \Delta), \tag{1}$$

where $\mathcal{F} = [F_x \ F_y \ M_z]^{\mathrm{T}}$ is the generalised force/moment applied to the COG, and can also be regarded as pseudo-control input.

One now needs to define $\mathcal{F}$, which depends on complex nonlinear friction forces generated in the tyre–road interface. To this end, it is convenient to first introduce some auxiliary variables: the linear velocities of the car (v_x, v_y), specified in the *xy* frames, and its yaw-rate $(\dot{\psi})$ can be obtained applying a change of coordinates between the *xy* and *XY* frames as

$$[v_x \ v_y \ \dot{\psi}]^{\mathrm{T}} = \mathbf{T}^{-1}(\mathbf{p})\dot{\mathbf{p}}. \tag{2}$$

Similarly, given that the wheels speeds are the consequence of the superposition of (v_x, v_y) and rotational motion (yaw-rate), one can write [29]

$$\begin{bmatrix} v_{Li} \\ v_{Ci} \end{bmatrix} = \mathbf{W}^{-1}(\delta_i) \begin{bmatrix} 1 & 0 & \chi_{Li} \\ 0 & 1 & \chi_{Ci} \end{bmatrix} \begin{bmatrix} v_x \\ v_y \\ \dot{\psi} \end{bmatrix}, \quad i \in \{1l, 1r, 2l, 2r\},$$

$$[\chi_{L1l} \ \chi_{L1r} \ \chi_{L2l} \ \chi_{L2r}] = \left[-\frac{c}{2} \ \frac{c}{2} \ -\frac{c}{2} \ \frac{c}{2} \right]; [\chi_{C1l} \ \chi_{C1r} \ \chi_{C2l} \ \chi_{C2r}] = [a \ a \ -b \ -b],$$

where (a, b) is the CoG position, c is the track width, δ_i is the steering angle of each wheel and $\mathbf{W}(\delta)$ denotes a change of coordinates between the vehicle local coordinates (xy) and the tyre LC frames, i.e.

$$\mathbf{W}(\delta) = \begin{bmatrix} \cos(\delta) & -\sin(\delta) \\ \sin(\delta) & \cos(\delta) \end{bmatrix}. \tag{3}$$

As depicted in Figure 2, the L component is aligned with the wheel longitudinal direction, while the C component points in the 'cornering' direction, orthogonal to the wheel L axis. To express the load transfer between the front–rear axle, and left–right wheels, a quasi-static mapping is used

$$\mathbf{F}_z = \mathbf{F}_z^0 + \mathbf{A}_x a_x + \mathbf{A}_y a_y,$$

$$\mathbf{F}_z = [F_{z1l} \ F_{z1r} \ F_{z2l} \ F_{z2r}]^{\mathrm{T}}, \quad \mathbf{F}_z^0 = \frac{mg}{2(a+b)}[b \ b \ a \ a]^{\mathrm{T}}, \tag{4}$$

$$\mathbf{A}_x = \frac{mh}{2(a+b)}[-1 \ -1 \ 1 \ 1]^{\mathrm{T}}, \quad \mathbf{A}_y = \frac{mh}{c(a+b)}[-b \ b \ -a \ a]^{\mathrm{T}},$$

where $\mathbf{F}_z^0$ is the static force distribution, h the height of the CoG, g the gravitational acceleration and a_x, a_y the longitudinal and lateral acceleration. The generalised forces/moments ($\mathcal{F}$) applied to the CoG is the aggregated result of the individual friction forces generated at the tyre–road interface, namely

$$\mathcal{F} = \mathbf{B}\mathbf{F}^{xy}, \quad \mathbf{B} = \begin{bmatrix} B_x \\ B_y \\ B_\psi \end{bmatrix} = \begin{bmatrix} 1 & 0 & 1 & 0 & 1 & 0 & 1 & 0 \\ 0 & 1 & 0 & 1 & 0 & 1 & 0 & 1 \\ -\frac{c}{2} & a & \frac{c}{2} & a & -\frac{c}{2} & -b & \frac{c}{2} & -b \end{bmatrix},$$

where $\mathbf{F}^{xy}$ are the friction forces of each tyre, defined in the xy frame (Figure 2):

$$\mathbf{F}^{xy} = [F_{x1l} \ F_{y1l} \ F_{x1r} \ F_{y1r} \ F_{x2l} \ F_{y2l} \ F_{x2r} \ F_{y2r}]^{\mathrm{T}}.$$

Given that the friction forces are usually represented in the LC wheel coordinate frame,[30] it is also helpful to decompose $\mathbf{F}^{xy}$ in the L and C components

$$\mathbf{F}^{xy} = \mathcal{W}(\delta)\mathbf{F}^{LC},$$

$$\mathcal{W}(\delta) = \begin{bmatrix} \mathbf{W}(\delta_{1l}) & \mathbf{0} & \mathbf{0} & \mathbf{0} \\ \mathbf{0} & \mathbf{W}(\delta_{1r}) & \mathbf{0} & \mathbf{0} \\ \mathbf{0} & \mathbf{0} & \mathbf{W}(\delta_{2l}) & \mathbf{0} \\ \mathbf{0} & \mathbf{0} & \mathbf{0} & \mathbf{W}(\delta_{2r}) \end{bmatrix}, \tag{5}$$

where $\mathbf{F}^{LC} = [F_{L1l} \ F_{C1l} \ F_{L1r} \ F_{C1r} \ F_{L2l} \ F_{C2l} \ F_{L2r} \ F_{C2r}]^{\mathrm{T}}$, and $\delta = [\delta_{1l} \ \delta_{2r} \ \delta_{2l} \ \delta_{2r}]^{\mathrm{T}}$ represent the steering angles. To model the friction forces $\mathbf{F}^{LC}$, a simplified version of the well-known magic tyre formula (MTF) will be used.[30] The main inputs for this model are: (i) the longitudinal tyre slip κ_i, a normalised difference between the wheel rotation speed (ω_i) and the wheel linear speed (v_{Li}) and (ii) the tyre side-slip angle α_i. Formally, these are defined as

$$\kappa_i = \frac{\omega_i r_i - v_{Li}}{v_{Li}}, \quad \tan\alpha_i = -\frac{v_{Ci}}{v_{Li}}, \tag{6}$$

where r_i is its effective radius, $i \in \{1l, 1r, 2l, 2r\}$ and v_{Li}, v_{Ci} the longitudinal and cornering speed of the tyre. To incorporate the combined slip conditions, the so-called 'theoretical slips'

[30] are considered, i.e.

$$\sigma_{Li} = \frac{\kappa_i}{1 + \kappa_i}, \quad \sigma_{Ci} = \frac{\tan\alpha_i}{1 + \kappa_i}, \quad \sigma_i = \sqrt{\sigma_{Li}^2 + \sigma_{Ci}^2}, \tag{7}$$

which represents the main factors in generating the longitudinal (F_{Li}) and cornering forces (F_{Ci}):

$$F_{Li} = \frac{\sigma_{Li}}{\sigma_i} F_i(\sigma_i, F_{zi}), \quad F_{Ci} = \frac{\sigma_{Ci}}{\sigma_i} F_i(\sigma_i, F_{zi}), \tag{8}$$

$$F_i(\sigma_i, F_{zi}) = F_{zi} D \sin(C \operatorname{atan}(B\sigma_i)), \tag{9}$$

where D, C, B are parameters of the model. Notice that, for simplicity, the representation of the tyre–road friction forces assumes an isotropic model. Furthermore, from Equations (8) and (9), it can be readily verified that the model satisfies

$$F_{Li}^2 + F_{Ci}^2 = F_i^2 \leq D^2 F_{zi}^2, \tag{10}$$

which is known as the friction circle constraint. Finally, the wheel rotational dynamics is given by

$$J\dot{\omega}_i = T_i - r_i F_{Li},$$

where J is the wheel inertia and T_i the wheel torque. Since the wheel rotational dynamics are, in general, much faster than the vehicle dynamics, the previous relations will be approximated with their steady-state relation, i.e.

$$F_{Li} = rT_i. \tag{11}$$

To model the drivers' inputs, it is assumed that the vehicle has front steer only, controlled by the driver, and the front steer angles are equal, that is

$$\delta_{1l} = \delta_{1r} = \delta_1; \quad \delta_{2l} = \delta_{2r} = 0. \tag{12a}$$

Furthermore, it is assumed that the torque applied to each wheel of the EV can be manipulated independently, and the summation of the wheels torques (u_T)

$$T_{1l} + T_{1r} + T_{2l} + T_{2r} = u_T \tag{13}$$

is imposed by the driver or by a high-level vehicular controller.

3. Baseline optimal solution

The definition of the benchmark optimal problem for the torque distribution strategy is now studied, the solution of which will enable us to extract the maximum performance from the WIMs. To this aim, an optimal control problem will be formulated, intended to move, in minimum time, the EV from an initial point $\mathbf{p}_0 = (X_0, Y_0, \psi_0)$ to a final point $\mathbf{p}_f = (X_f, Y_f, \psi_f)$, while fulfilling the physical constraints given by the road grip capabilities (see, e.g. Figure 3 for an illustration of a typical setting to negotiate a $90°$ corner).

3.1. *Time–distance transformation*

Consider the equation of motion re-written as a first-order differential-algebraic equation of the form

$$\frac{\mathrm{d}\mathbf{z}_1}{\mathrm{d}t} = \mathbf{z}_2, \tag{14a}$$

$$\mathbf{M}\frac{\mathrm{d}\mathbf{z}_2}{\mathrm{d}t} = \mathbf{T}(\mathbf{z}_1)(\mathcal{F} - \Delta), \tag{14b}$$

where $\mathbf{z}_1 = \mathbf{p}$ is the position, $\mathbf{z}_2 = \mathrm{d}\mathbf{p}/\mathrm{d}t$ the velocity and t the independent variable. A common technique when dealing with minimum-time problems is to introduce the spatial coordinate s as an independent variable. There are several advantages in adopting this change of variable. First, unlike the time, the use of the distance s as an independent variable allows us to fix its final value, which is particularly useful when discretising the optimisation problem.[23] Secondly, the distance is also a natural variable to parameterise the road boundaries (as will be shown in the following), and the incorporation of the road constraints in the problem is greatly simplified using s as an independent variable. Finally, if long routes need to be considered, the problem can be decomposed into shorter sectors and, this, albeit yielding sub-optimal results, is normally much easier to solve than the original global problem.

In the sequel, s is the one-dimensional position of the vehicle along the road (Figure 3); it is measured and normalised so that $s = 0$ at the beginning of the road and $s = 1$ at the end of the road. The increments of time t and spatial coordinate s are related as

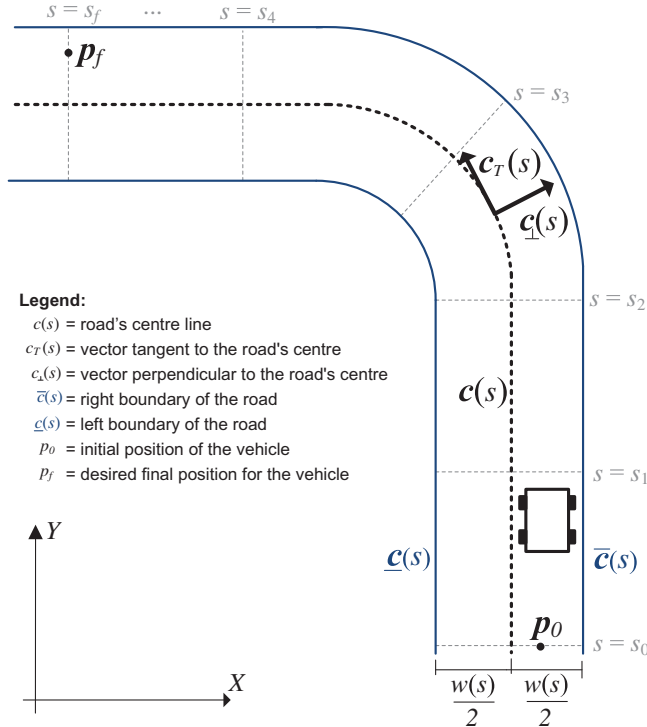$$\dot{s}\,\mathrm{d}t = \mathrm{d}s, \tag{15}$$

Figure 3. Definition of the road centre, road boundaries and auxiliary variables.

where $\dot{s} = f_s(\mathbf{z}_1, \mathbf{z}_2, s)$ is a normalised speed, the definition of which is postponed to Section 3.3. Inserting the previous relation into Equation (14), one has

$$\frac{d\mathbf{z}_1}{ds} = \frac{1}{\dot{s}}\mathbf{z}_2, \tag{16a}$$

$$\mathbf{M}\frac{d\mathbf{z}_2}{ds} = \frac{1}{\dot{s}}\mathbf{T}(\mathbf{z}_1)(\mathcal{F} - \Delta), \tag{16b}$$

which is a scaled version of the original dynamics. Similarly, the total time of the manoeuvre (T) can be obtained as

$$T = \int_0^T dt = \int_0^{\bar{s}} \frac{1}{\dot{s}}\,ds, \tag{17}$$

where $\bar{s}$ is the total length of the track.

3.2. *Road definition and boundaries*

One of the requirements that must be incorporated in the problem formulation is the track constraint, i.e. the vehicle must be, at all times, within the road boundaries. To simplify the analysis, it will be assumed that it is enough to keep only the vehicle CoG within the road boundaries. To formally characterise the road, consider that the coordinates of the road centre line are known and defined through the two-dimension vector $\mathbf{c}(s) = (c_X(s), c_Y(s)) \in \mathbb{R}^2$, parameterised as a function of the path coordinate s. From this, the vectors tangent ($\mathbf{c}_T(s)$) and parallel ($\mathbf{c}_\perp(s)$) to the road centre can be readily computed, as illustrated in Figure 3. Next, assuming that the distance between the track centre and the road boundaries is $\pm w(s)/2$, the lower and upper bounds of the road can be expressed as

$$\bar{\mathbf{c}}(s) = \mathbf{c}(s) + \frac{w(s)}{2}\frac{\mathbf{c}_\perp(s)}{\|\mathbf{c}_\perp(s)\|}, \quad \underline{\mathbf{c}}(s) = \mathbf{c}(s) - \frac{w(s)}{2}\frac{\mathbf{c}_\perp(s)}{\|\mathbf{c}_\perp(s)\|}, \tag{18}$$

where $\|\cdot\|$ is the Euclidean norm. Following a similar methodology to the one described in [31], the track constraints can now be formulated as a set of linear equalities and inequalities of the form

$$\mathbf{c}_\perp(s)^{\mathrm{T}}(\mathbf{Pz}_1(s) - \bar{\mathbf{c}}(s)) \leq 0, \quad -\mathbf{c}_\perp(s)^{\mathrm{T}}(\mathbf{Pz}_1(s) - \underline{\mathbf{c}}(s)) \leq 0, \tag{19a}$$

$$\mathbf{c}_T(s)^{\mathrm{T}}(\mathbf{Pz}_1(s) - \mathbf{c}(s)) = 0, \quad \mathbf{P} = \begin{bmatrix} 1 & 0 & 0 \\ 0 & 1 & 0 \\ 0 & 0 & 0 \end{bmatrix}. \tag{19b}$$

The first two inequalities state that, for a given s, the position of the vehicle CoG should not exceed the lower and upper bounds of the road, while the last constraint imposes that $\mathbf{z}_1$ should lie within the road boundaries. For a fixed $s = s_i$, the intersection of these three constraints produces a straight line, which can be regarded as a 'wayline' that the vehicle should pass (see the grey lines s_i plotted in Figure 3).

3.3. *Problem formulation and solution*

It is now possible to formulate the benchmark optimisation problem:

$$
\min_{\dot{s}, \mathbf{z}_1, \mathbf{z}_2, T_i, \delta_1} \quad \int_0^{\bar{s}} \frac{1}{\dot{s}} \, \mathrm{d}s
$$

$$
\begin{aligned}
\text{s.t.} \quad & (16), \; \dot{s} = f_s(\mathbf{z}_1, \mathbf{z}_2, s), \quad \dot{s} > 0, \quad s \in [0, \bar{s}] \\
& (19), \; \mathcal{F} = f_F(\mathbf{z}_1, \mathbf{z}_2, T_{1l}, T_{1r}, T_{2l}, T_{2r}, \delta_1) \\
& \mathbf{z}_1(0) = \mathbf{p}_0, \quad \mathbf{z}_1(\bar{s}) = \mathbf{p}_f, \quad \mathbf{z}_2(0) = [\dot{X}_0 \; \dot{Y}_0 \; \dot{\psi}_0]^{\mathrm{T}} \\
& |\delta_1| \le \overline{\delta}_F, \quad \underline{T} \le T_i \le \overline{T}, \quad i \in \{1l, 1r, 2l, 2r\},
\end{aligned}
\tag{20}
$$

where the first set of constraints is related with the vehicle's equations of motion; given that we are interested in minimum-time results, it was assumed that the vehicle (normalised) speed should be always positive, which also avoids a division by zero in Equation (16); the second set of constraints is concerned with the road boundaries and the friction force model; the function f_F is a nonlinear algebraic map, which results from aggregating Equations (2)–(12); the third set of constraints imposes the initial and final position of the vehicle, as well as its initial speed; the fourth/last set of constraints are due to the actuators saturation limits. In light of the nonlinearities present in Equation (20), mainly due to the friction force model, it is difficult to analytically establish the optimality conditions for the problem. Consequently, to ease the solution of this problem, a direct optimisation approach was adopted, also known as the transcription formulation.[32,33] This means that the dynamic equations in (20) were discretised (in this work through the Euler forward method), yielding a large nonlinear optimisation problem that was solved with the help of the ipopt solver.[34] Finally, to avoid numerical issues due to different magnitudes of the variables, the final formulation of the discrete optimisation problem employed uniformly scaling factors for all the decision variables, see [33, p.166].

The discretisation of the optimisation problem also brings in an interesting simplification in the computation of $\dot{s}$. In fact, although one may determine $f_s(\cdot)$ in continuous time (see, e.g. [35]), the discrete version is not only simpler, but also more intuitive. To see this better, let us consider that the vehicle CoG is at the position $\mathbf{z}_1(s_i)$, with velocity $\mathbf{z}_2(s_i)$, and that it reaches, after one integration step, the position $\mathbf{z}_1(s_{i+1})$. Assuming the forward Euler discretisation, one can approximate $\dot{s}[s_{i+1}]$ as

$$
\dot{s}[s_{i+1}] \approx \frac{s_{i+1} - s_i}{\Delta t} = (s_{i+1} - s_i) \frac{\|\mathbf{P}\mathbf{z}_2(s_i)\|}{\|\mathbf{P}(\mathbf{z}_1(s_{i+1}) - \mathbf{z}_1(s_i))\|}.
$$

Replacing this approximation in the total manoeuvre time one has

$$
T = \int_0^{\bar{s}} \frac{1}{\dot{s}} \, \mathrm{d}s \approx \sum_{i=0}^{N-1} \frac{\|\mathbf{P}(\mathbf{z}_1(s_{i+1}) - \mathbf{z}_1(s_i))\|}{\|\mathbf{P}\mathbf{z}_2(s_i)\|} (s_{i+1} - s_i),
\tag{21}
$$

which reveals that, to minimise the time T, the vehicle speed ($\|\mathbf{P}\mathbf{z}_2\| = \sqrt{\dot{X}^2 + \dot{Y}^2}$) should be maximised and the travelled distance between successive 'waylines' ($\|\mathbf{P}(\mathbf{z}_1(s_{i+1}) - \mathbf{z}_1(s_i))\| = \sqrt{(X(s_{i+1}) - X(s_i))^2 + (Y(s_{i+1}) - Y(s_i))^2}$) should be as low as possible. This analysis is in accordance with the traditional approach of racing drivers, which normally try to 'cut the corners' (thus minimising the travelled distance) with the maximum possible speed. Of course, the expression for $\dot{s}$ presented above can be straightforwardly adapted to other discretisation schemes.
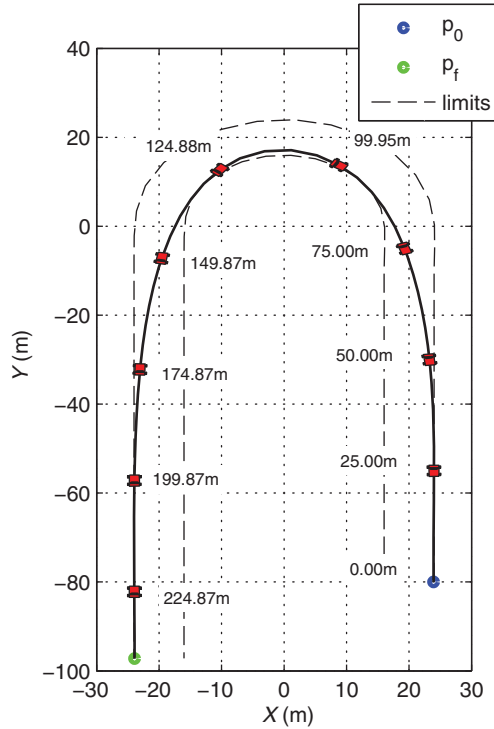
Figure 4. Optimal trajectory for the harping corner.

3.4. *Example*

To illustrate the results that can be obtained with the approach introduced above, Figures 4 and 5 present the optimal solution for negotiating a hairpin corner, with a radius of 20 m and initial speed of 100 km/h. The vehicle parameters are reported in Appendix 1, while the sampling distance employed in the discretisation was 5 m. Analysing Figure 5, one can see that for $s \in [20, 70]$ m the vehicle is decelerated, with the front WIMs providing the majority of the braking torque; due to the rear-to-front load movement, this is a reasonable allocation solution. Furthermore, for $s \in [70, 110]$ m, the vehicle enters the corner, and the driver applies combined steering and braking. It is worth noticing that, to maximise the lateral force (F_y) along this road segment, the (expert) driver increases the steering angle and gradually releases the brake pedal (see the plots of δ_1 and u_T, respectively). A dual situation occurs at the corner exit, $s \in [110, 140]$ m, with the gradual reduction of the steering angle and a smooth increase in the applied torque.

Remark 3.1 The optimal results for the harping corner reveal that, for most of the time, the external wheels (front right and rear right, in this specific example) receive a larger torque than the inner ones, i.e. $|T_{1r}| \geq |T_{1l}|, |T_{2r}| \geq |T_{2l}|$. This means that, during combined braking and steering, the torque allocation is generating an 'understeering yaw-moment' (see ΔM_z in Figure 5), while an 'oversteering yaw-moment' is produced during combined acceleration and steering. From a friction use point-of-view such an allocation is reasonable as, in practice, larger torque is applied to the wheels that experience a larger vertical load.
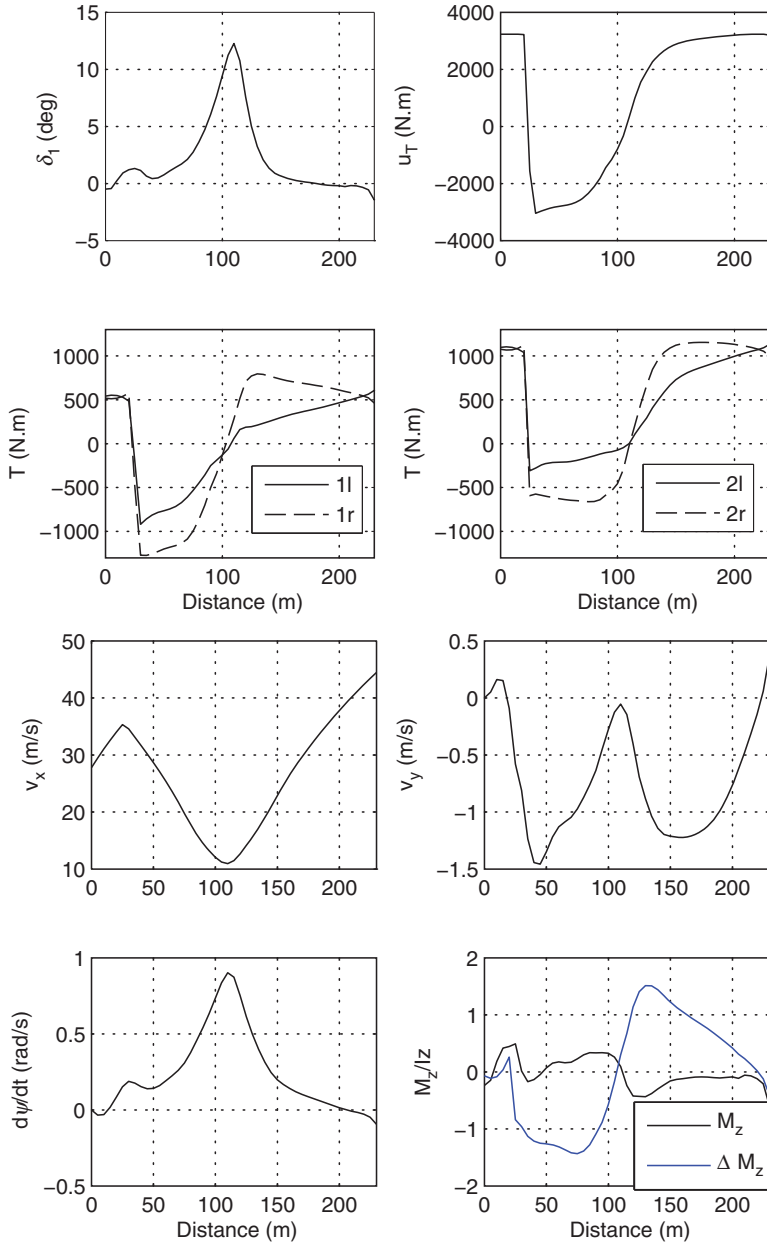
Figure 5. Baseline solution for the hairpin corner manoeuvre: ΔM_z represents the (additional) yaw-moment generated by the torque split in the WIMs.

Remark 3.2 The min-time torque allocation solution suggests that, in order to achieve the full performance of the vehicle, the driver will have to cope with understeering in the corner entry and oversteering in corner exit.

To better explain the previous remark, let us look more closely at the results depicted in Figure 5. First, notice that in the initial part of the manoeuvre $s \in [0, 110]$ m, the (ideal) driver applies a positive steering in order to approach the left-hairpin corner, which then results in a positive (steering) yaw-moment and an increase in the yaw-rate (see bottom plots
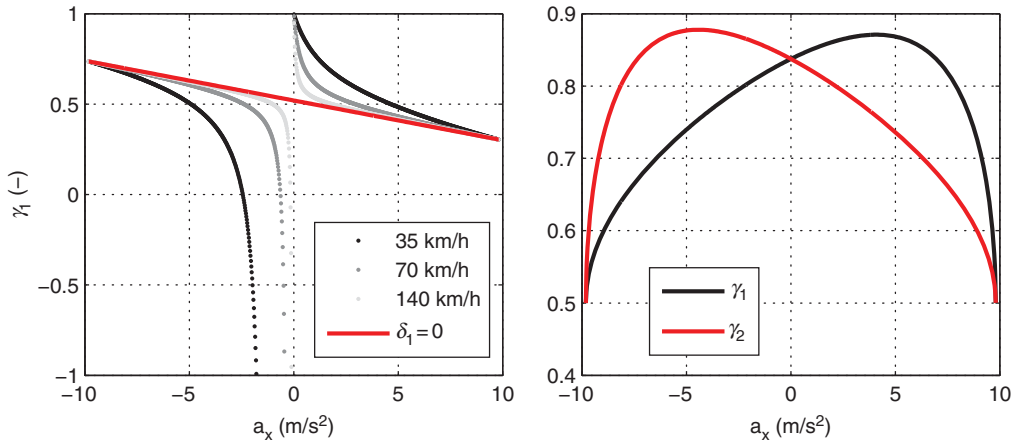
Figure 6. Torque allocation ratios when the vehicle is operating close to the friction limit. To simplify the graphical representation only the case with $a_y \geq 0$ is shown, and the γ_0 plot was computed assuming $\delta_1 = a_y(a+b)/V^2$.

of Figure 6). However, during the same period, one can also observe that the differential left/right braking torque is contributing with a negative yaw-moment, $\Delta M_z < 0$ (see also Remark 3.1). This means that the yaw-moment generated by the torque difference in the left/right wheels is opposing the yaw-moment generated by the car steering. Consequently, in this left-harping corner, the driver is turning the steering to the left side, but the torque difference in left/right wheels is 'pulling' the car to the right side of the track. To compensate this effect, the driver will have to apply more steer, which will make him feel that the car is 'understeering' and, perhaps, regard this as an degradation (a dual situation happens in the corner exit, [110–200] m, but, in this case, featuring 'oversteering'). In any case, since the EV is being driven by an 'ideal driver', i.e. the steering angle is generated by an optimisation framework, these potential imbalances are not relevant here.

4. Causal torque allocation strategy

The methodology described in the previous section is a valuable tool to gain some insight on the optimal torque allocation for the WIMs. However, in practice, this approach is not appropriate for real-time implementation because, in addition to the high computational burden, the vehicle trajectory cannot in general be assumed to be known in advance. Thus, we aim at emulating the previous baseline optimal solution in a real-time environment with causality constraints. This led to devise a causal torque allocation strategy that, assuming knowledge of the driver's inputs (δ_1, u_T) and of the vehicle speed and accelerations (v_x, a_x, a_y), produces as output the wheel torque references $T_{1l}, T_{1r}, T_{2l}, T_{2r}$ capable of exploiting the full potential of the WIMs.

4.1. Allocation ratios

To facilitate the design of the allocator, three normalisation factors are introduced (γ_0, γ_1, γ_2) which, together with u_T, parameterise the torque distribution

$$
\begin{aligned}
T_{1l} &= u_T\gamma_0(1-\gamma_1) & T_{1r} &= u_T\gamma_0\gamma_1, \\
T_{2l} &= u_T(1-\gamma_0)(1-\gamma_2) & T_{2r} &= u_T(1-\gamma_0)\gamma_2,
\end{aligned}
\tag{22}
$$

where γ_0 is the front/rear allocation ratio ($\gamma_0 = 1$ means all the torque is applied to the front axle); γ_1 is the left/right allocation ratio of the front axle ($\gamma_1 = 1$ means all the front axle torque is on the right wheel); γ_2 is the left/right allocation ratio of the rear axle. Notice that, in conventional vehicles, the ratio γ_0 is a well-known quantity for distributing the braking force among the axles [36]; our idea here is to generalise this concept for the left/right torque split in the front and rear axles.

4.2. *Allocator design*

The torque allocation problem, as stated above, has been previously addressed in the literature.[24–26] These studies assume that the vehicle is operating close to the quasi-steady-state (QSS) conditions, i.e. constant accelerations and constant yaw-rate, which simplifies the analysis of the nonlinear vehicle model. Based on the QSS conditions, the torque allocation problem is then formulated within an optimisation framework, aiming to maximise the longitudinal acceleration for constant radius cornering [25] or the CoG force in an arbitrary direction.[24] In what follows, these results will be reformulated and extended in two directions. First, the theoretical results proposed in [24,26] will be examined in light of the ratios defined in Equation (22), which will put in evidence the important role that the vertical forces (F_z) have in the torque distribution. Secondly, while the studies [24,26] focus mainly on investigating the impact that WIMs have on the vehicle operation envelope (i.e. on the gg diagram), we will go one step further, and devise a torque allocation strategy that can be implemented in real-time.

To do that, it is worth noting that, while the baseline solution presented in the previous section seeks the minimisation of the manoeuvre time, this cost function is not appropriated for devising a causal allocation strategy, as it asks to know the manoeuvre itself in advance. To overcome this limitation, here a different performance metric will be explored, suitable for real-time implementation, but which, from a manoeuvre-time perspective, only ensures sub-optimal results. The idea behind the sub-optimal formulation is largely inspired by the gg-diagram concept, a tool that generalises the tyre friction circle concept to the vehicle CoG forces/accelerations.[37] It is well known in the racing community that, in order to minimise the lap-time, the vehicle should operate close to the boundaries of the gg-diagram. With this idea in mind, the design of the causal torque allocator will seek to maximise the CoG forces (F_x, F_y) applied to the vehicle in a given direction (inferred from the current vehicle state). This strategy will promote the maximisation of the vehicle performance envelope, which in turn will enable the driver to reduce the manoeuvre time.

To design the torque allocator, it is convenient to consider the CoG forces represented in polar coordinates, i.e. $F_x + \mathrm{j}F_y = \rho e^{\mathrm{j}\phi}$, where ρ is the force magnitude and ϕ the force angle in relation to the x-axis. It will be assumed that the vehicle is operating under QSS conditions (i.e. constant longitudinal, lateral and yaw accelerations), and that the desired force angle ϕ is fixed and known (note that the force direction can be straightforwardly inferred from the current value of a_x and a_y). The goal is to find the tyre forces $\mathbf{F}^{xy}$ that maximise the force magnitude ρ in the direction ϕ. More specifically, this problem can be formulated as

$$\min_{\rho, \mathbf{F}^{xy}} \quad -\rho$$

$$\text{s.t.} \quad \mathbf{B}_x^{\mathrm{T}}\mathbf{F}^{xy} - \rho \cos(\phi) = 0; \quad \mathbf{B}_y^{\mathrm{T}}\mathbf{F}^{xy} - \rho \sin(\phi) = 0; \quad \mathbf{B}_\psi^{\mathrm{T}}\mathbf{F}^{xy} = 0 \tag{23}$$

$$(\mathbf{C}_i^{\mathrm{T}}\mathbf{F}^{xy})^2 + (\mathbf{D}_i^{\mathrm{T}}\mathbf{F}^{xy})^2 \leq \left(\overline{\mu}\mathbf{E}_i^{\mathrm{T}}\left(\mathbf{F}_z^0 + \mathbf{A}_x\frac{\rho}{m}\cos(\phi) + \mathbf{A}_y\frac{\rho}{m}\sin(\phi)\right)\right)^2,$$

where $i = \{1l, 1r, 2l, 2r\}$, and $\mathbf{B}_x, \mathbf{B}_y, \mathbf{B}_\psi$ are the matrices that compose $\mathbf{B}$ in Equation (5). In the above optimisation problem, the first two constraints ensure that the force applied to CoG is applied in the desired direction, while the third constraint is related with the constant yaw-rate assumption (resulting from the QSS conditions) the fourth constraint takes into account the restrictions introduced by the friction circle, defined in Equation (10), where $\mathbf{C}_i, \mathbf{D}_i, \mathbf{E}_i$ are the matrices that extract the x, y and z force component for each tyre.

Although the previous problem can be solved numerically, Klomp [24] presented a very useful analytical solution in

LEMMA 4.1 see [24]   *Consider the forces of each tyre, defined in the xy-axis:* $F_{xi} + jF_{xi} = \rho_i e^{j\phi_i}$. *Assuming that* (i) *the orientation of the tyre forces coincides with the orientation of the CoG force, i.e.* $\phi_i = \phi$; (ii) *the wheels operate at the limit of adherence:* $\rho_i = \mu F_{zi}$, *the solution to Equation* (23) *is given by*

$$\begin{bmatrix} F_{xi} \\ F_{yi} \end{bmatrix} = \overline{\mu} F_{zi} \begin{bmatrix} \cos(\phi) \\ \sin(\phi) \end{bmatrix} = \overline{\mu} \mathbf{E}_i^{\mathrm{T}} (\mathbf{F}_z^0 + \mathbf{A}_x \frac{\rho}{m} \cos(\phi) + \mathbf{A}_y \frac{\rho}{m} \sin(\phi)) \begin{bmatrix} \cos(\phi) \\ \sin(\phi) \end{bmatrix}.$$

Since our ultimate goal is to determine the WIM torques, and in view of the linear relation between torque and longitudinal force expressed by Equation (11), it is desirable to transform the forces $\mathbf{F}^{xy}$, defined in the above Lemma, to the *LC* coordinate system, fixed to the wheel. Accordingly, combining Equations (24) and (5) one obtains

$$F_{Li} = \overline{\mu} F_{zi} (\cos(\delta_i) \cos(\phi) + \sin(\delta_i) \sin(\phi)), \tag{24a}$$

$$F_{Ci} = \overline{\mu} F_{zi} (- \sin(\delta_i) \cos(\phi) + \cos(\delta_i) \sin(\phi)). \tag{24b}$$

Combining the previous equations with Equations (11) and (22), the allocation ratios can be determined as

$$\gamma_0 \approx \left(1 + \frac{a_x}{a_x \cos(\delta_1) + a_y \sin(\delta_1)} \frac{F_{z2l} + F_{z2r}}{F_{z1l} + F_{z1r}} \right)^{-1}, \tag{25a}$$

$$\gamma_1 = \frac{rF_{L1r}}{rF_{L1f} + rF_{L1r}} = \frac{F_{z1r}}{F_{z1r} + F_{z1l}}, \quad \gamma_2 = \frac{rF_{L2r}}{rF_{L2f} + rF_{L2r}} = \frac{F_{z2r}}{F_{z2r} + F_{z2l}}. \tag{25b}$$

Notice that, during the derivation of Equation (25a), the force direction ϕ was inferred from the vehicle acceleration: $ma_x \approx \rho \cos(\phi)$, $ma_y \approx \rho \sin(\phi)$. Inspecting the above formulas, it is worth pointing out that γ_1 and γ_2 (left/right allocation ratios) are not directly affected by the force direction (ϕ) or by the steering angle. Actually, they only depend on the ratio of the vertical forces, which generates fairly intuitive allocation results: (i) during straight line manoeuvres, equal torques are applied to the wheels of the same axle;[1] (ii) during cornering, the outside wheel receives more torque than the inside one (lighter wheel), in accordance with the left–right and front–rear weight shift that affects the vehicle. It is also interesting to note that all ratios are independent of the tyre–road friction peak $\overline{\mu}$.

Since the tyres vertical forces are intrinsically related with the longitudinal and lateral accelerations, cf. Equation (4), the torque ratios can also be expressed in the following equivalent form:

$$\gamma_0 = \left(1 + \frac{a_x}{a_x \cos(\delta_1) + a_y \sin(\delta_1)} \frac{ag + ha_x}{bg - ha_x} \right)^{-1}, \tag{26a}$$

$$\gamma_1 = \frac{(gb/2) - (h/2)a_x + (hb/c)a_y}{gb - ha_x}, \quad \gamma_2 = \frac{(ga/2) + (h/2)a_x + (ha/c)a_y}{gb + ha_x}. \tag{26b}$$
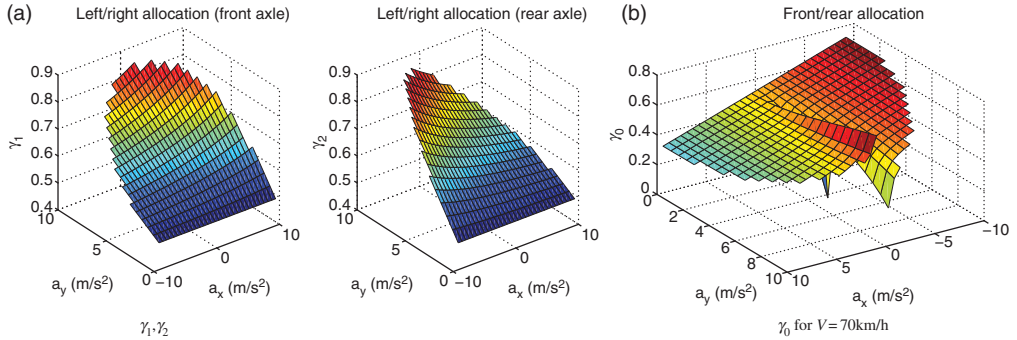
Figure 7. Torque allocation ratios when the EV is operating within the 'friction circle'. To simplify the graphical representation only the case with $a_y \geq 0$ is shown, and the γ_0 plot was computed assuming $\delta_1 = a_y(a + b)/V^2$.

Remark 4.2 If $\delta_1 = 0$, then Equation (26a) yields the ideal front/rear braking distribution (in the sense that the rear wheels will only lock after the front) employed in conventional vehicles.[36] This means that the above allocation strategy recovers the well-known front–rear braking distribution that ensures that the rear wheels only lock after the front.

To investigate the evolution of the front/rear ratio γ_0 with combined acceleration/ cornering, consider the allocation results illustrated in Figure 6. From these results, one can see that, as $|a_x|$ increases, γ_0 converges to the situation with $\delta_1 = 0$ (straight line allocation). On the other hand, for small longitudinal accelerations (almost pure cornering), there is a discontinuity in γ_0, being more pronounced at low speeds; since this discontinuity happens mainly when a_x is close to zero (thus the torque applied to the wheels is small), this is not a concern. Nonetheless, to avoid any numerical issue that may appear with the division-by-zero in Equation (25a), the final implementation of the allocator saturates the output of γ_0, so that this ratio lies always in the range $[-1, 1]$.

As for the evolution of γ_1, γ_2, one can observe that these variables always take values larger than 0.5, which implies that the allocator will generate an 'understeer' yaw-moment during braking (and an 'oversteer' during acceleration). These results are in accordance with the qualitative analysis of the baseline solution, discussed in Remark 3.1. Finally, it is worth noting that, although Equation (25) was determined assuming that the vehicle (and tyres) is operating at the boundary of adhesion conditions (see the second assumption considered in Lemma 4.1), nothing prevents us from extrapolating these expressions for other driving conditions. For example, Figure 7 shows the allocation ratios when the EV is operating within the friction limits. Based on this extrapolation, the final causal torque allocation used hereafter is expressed by the relations (25) and (22), which mainly depends on the vertical tyre load estimator. Although, in this work, a steady-state vertical load model has been adopted, it is worth pointing out that the causal torque allocation proposed in Equation (25) can also be implemented with a more complex vertical load representation, capable of capturing the suspension dynamics.

5. Evaluation of the allocator performance via simulation tests

In this section, a comparative study between the two allocations strategies discussed in the previous two sections will be carried out. The first allocation strategy, called baseline torque allocation solution, employs a discretised version of Equation (20) to determine the ideal
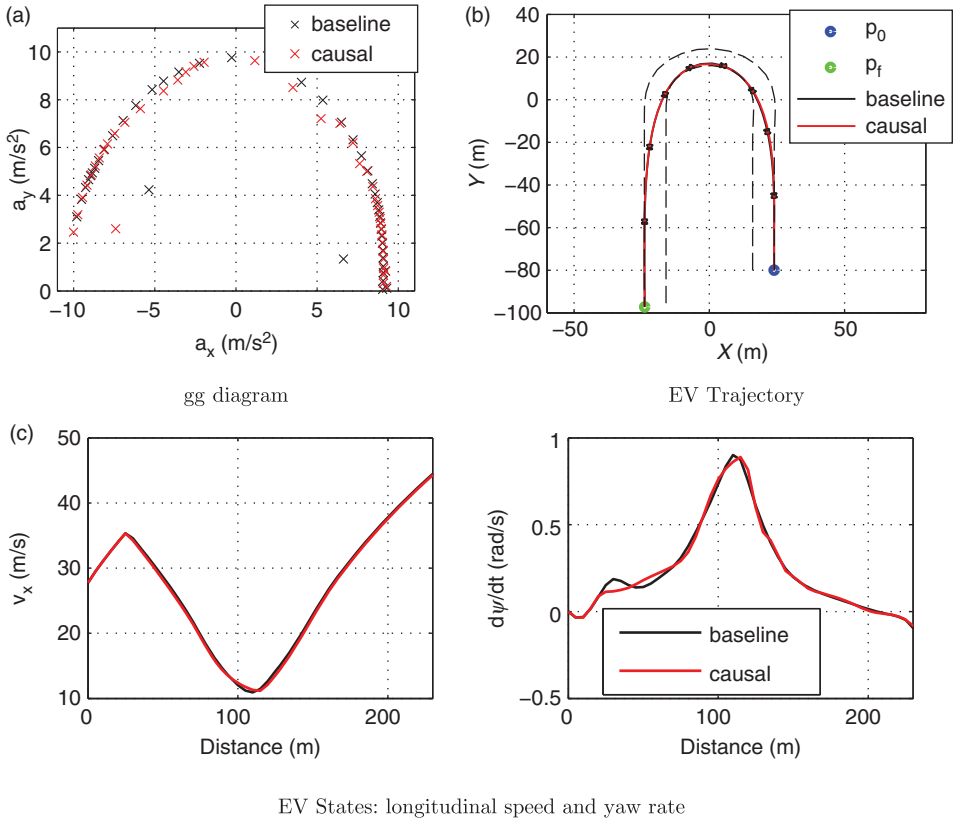
Figure 8. Simulation results for the hairpin corner: gg-plot, trajectory, speed and yaw-rate.

control inputs that allows the vehicle to execute a given manoeuvre in minimum time. In this case, the numerical solver explores five control inputs (front steer δ_1 + four wheel torques T_i, $i \in \{1l, 1r, 2l, 2r\}$) to achieve the minimum-time solution. The second allocation strategy under study, named causal torque allocation, employs Equation (20) subject to the additional constraints (25), which enables us to incorporate a fixed torque split policy in the optimisation problem. For this latter strategy, the numerical solver is only free to explore two control inputs (front steer δ_1 and torque summation u_T) to achieve the minimum-time solution. In other words, the evaluation of the causal allocation problem is taking advantage of the optimisation framework to emulate the 'ideal driver', which will minimise the manoeuvre time of the EV configured with a fixed torque split strategy. It is worth noting that the operation of the vehicle in the limit of adhesion (i.e. with 100% of friction potential) is only made possible by the use of an 'ideal driver' model, emulated through an optimisation framework, which will be able to cope with extreme driving conditions, such as saturated tyre forces, see also [22,35].

5.1. Hairpin corner

Figures 8–11 show the simulation results obtained for the hairpin corner, with an initial speed of 100 km/h and a corner radius of 20 m. Roughly speaking, it can be seen that both allocation strategies produce a trajectory, as well as driver inputs, longitudinal and rotational speeds, very similar to each other (see, in particular, Figures 8 and 9), which demonstrates

(a)

Driver inputs
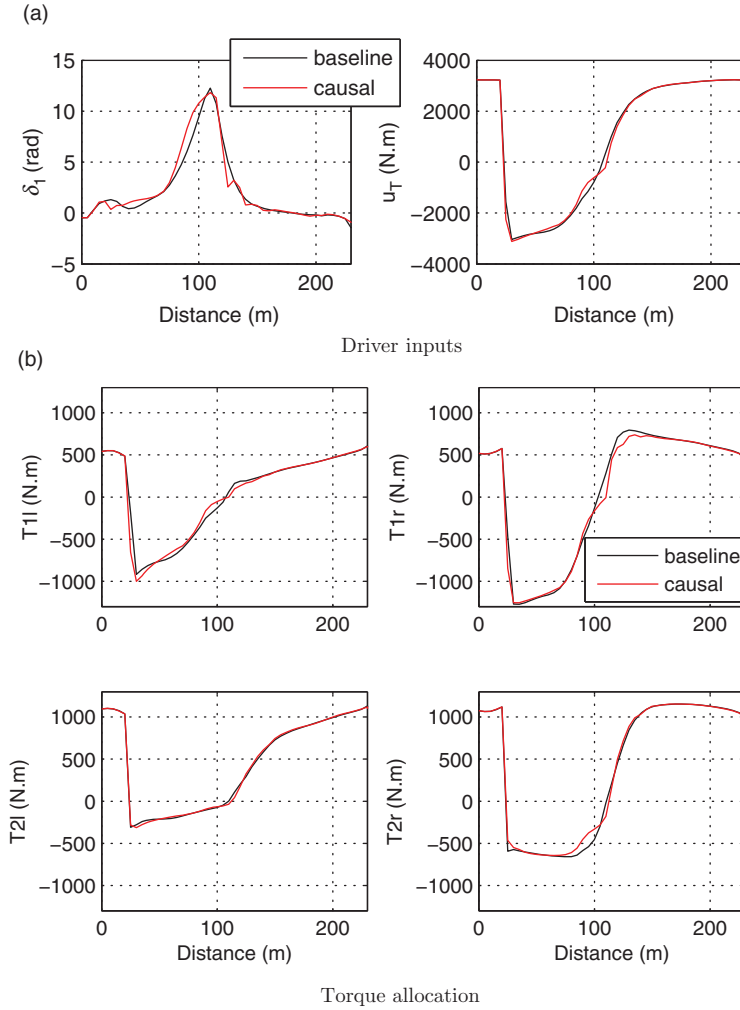
(b)

Torque allocation

Figure 9.   Simulation results for the hairpin corner: driver inputs and torques.

a very satisfactory performance of the causal allocation strategy. Nonetheless, there are also small differences that are worth discussing. For example, by inspecting the torque allocation ratios shown in Figure 10, one can find that the majority of the discrepancies are concentrated in the region $s \in [90, 120]$ m, which coincides with the situation where the vehicle is approaching the pure cornering situation. To explain the reason behind these discrepancies, recall that the causal allocation strategy was devised under the assumption that the EV is operating under QSS conditions, which assumes an almost constant yaw-rate. However, as we get closer to the pure-cornering situation, the QSS assumption gets weaker (see, e.g. the yaw-rate transient represented in Figure 8(c)), which leads to a slight degradation in the performance of the causal allocation. Another possible cause for the small discrepancies may be related with the singularity of the longitudinal accelerations, in manoeuvres in which such an acceleration tends to vanish. This degradation can be quantified in light of different criteria. From manoeuvre-time standpoint, the baseline approach requires 9.67 s, while the causal needs 9.75 s , meaning a degradation of only +0.8% of time. From the friction use perspective (see Figure 11), it can be observed that the causal allocation leaves some margin for use:
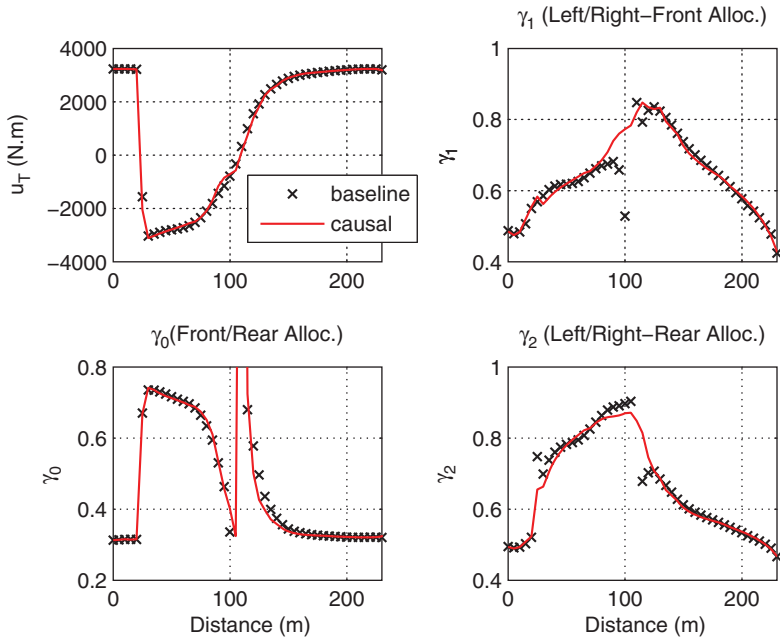
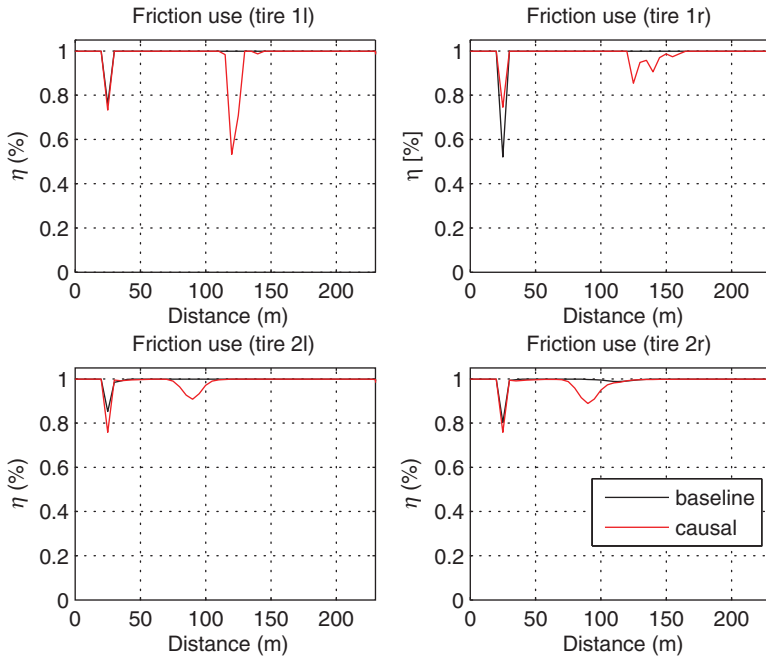Figure 10. Allocation ratios during the hairpin corner manoeuvre.

Figure 11. Friction use ($\eta_i^2 = (F_{Li}^2 + F_{Ci}^2)/(\overline{\mu}F_{zi})^2$) during the hairpin corner manoeuvre.

as the EV approaches the corner apex, the rear wheels decrease their friction utilisation to 90%, but recover the full friction use during the traction phase (the front wheels have a dual behaviour).
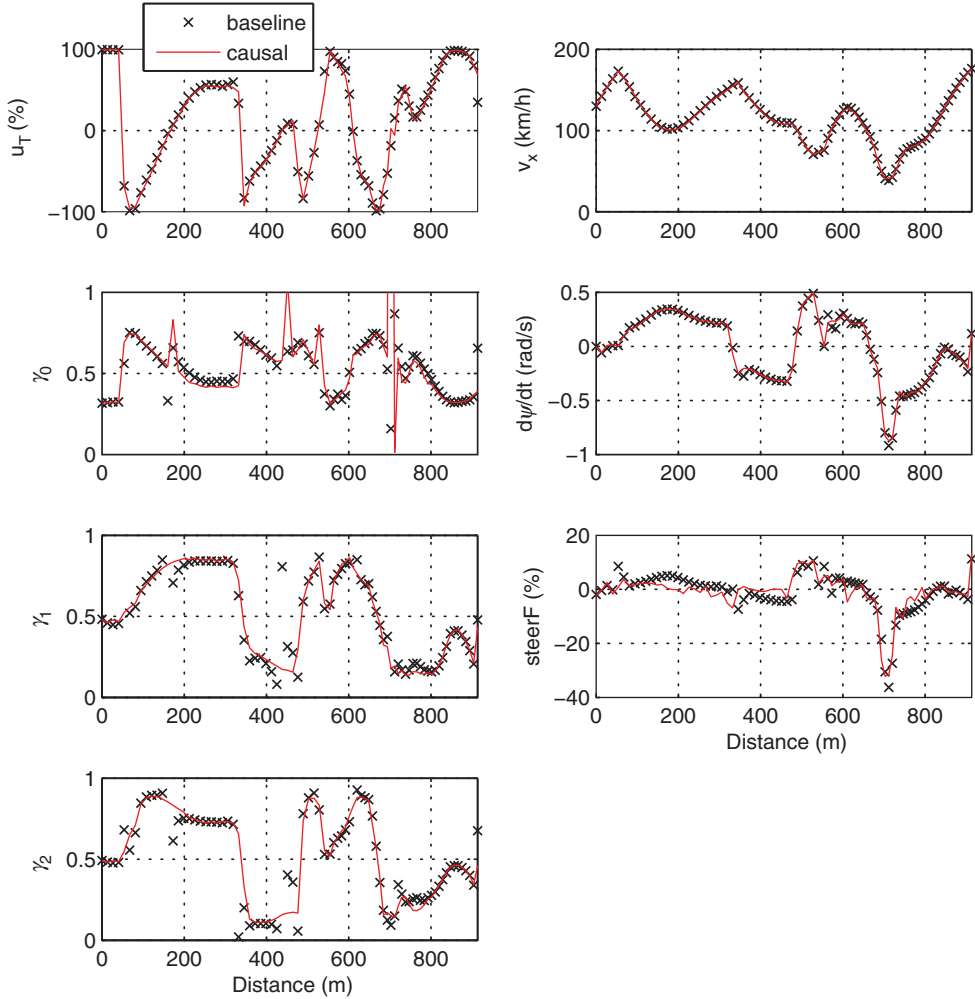
Figure 12. Driver inputs, vehicle states and torque allocation ratios for the road course simulation (for graphical convenience, the steering and throttle/braking pedal variables were normalised).

5.2. *Test-track*

To compare the allocation strategies in a more realistic setting, the last 900 m of the Monaco track was considered, as shown in Figure 12. Similar to the previous tests, one can verify that the causal allocation yields an evolution (driver inputs, vehicle states and allocation ratios) very close the baseline solution. This proximity between solutions is also reflected in the total manoeuvre time: 30.43 s for the baseline and 30.64 s (+0.70%) for the causal allocation.

Remark 5.1 [(Alternative vehicle configurations)] This work was focused on power train configuration having 4 WIMs and front steer (2 WS). Nonetheless, thanks to the optimal framework discussed in Section 3, we can easily adapt the baseline solution to tackle others power train configurations. To illustrate this feature, we carried out a performance comparison between the 4 WIMs + 2 WS and the following configurations:

- 4 WIMs + 4 WS, which is obtained by removing constraint (15b) from the optimisation problem, and introducing rear steer δ_2 (with same limits as the front steering).
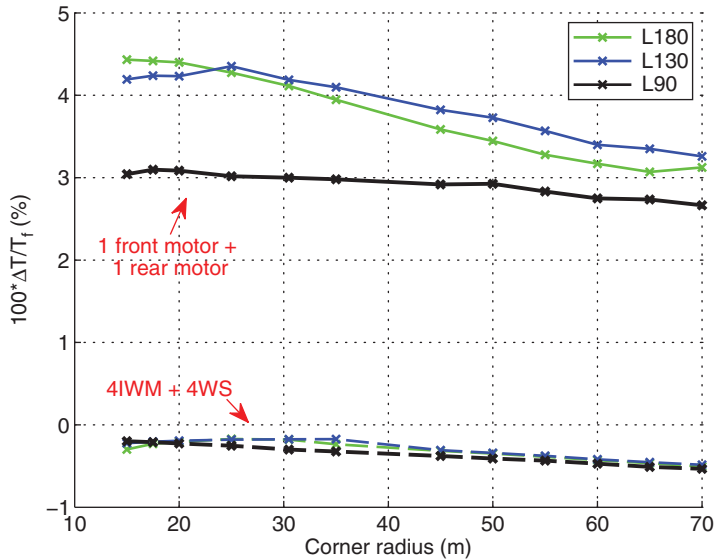
Figure 13. Comparison of the performance of different power train configurations: (i) 4 WIM + 2 WS (the baseline solution); (ii) 4 WIM + 4 WS and (iii) two electric motors connected, through open mechanical differentials, to each axle of the vehicle. The variable ΔT plotted on the y-axis (normalised with respect to the front torque T_f) is defined as $\Delta = T_{\text{baseline}} - T_{\text{causal}}$.

- Two centralised electric motors coupled, through open mechanical differentials, to each axle of the vehicle, i.e. $T_{1f} = T_{1r}, T_{2f} = T_{2r}$.

Figure 13 depicts the normalised time difference that occurs with the aforementioned vehicular configurations to negotiate a 180°, 130° and 90° corners in minimum time . From these results, one can conclude that the use of 4 WS (with 4 WIMs) only contributes to a slight decrease in the manoeuvre time (-0.5%), which demonstrates that the configuration under investigation in this work (4 WIM + 2 WS) is capable of extracting almost the full potential available in the vehicle. Furthermore, one can also find that the use of two-centralised electric motors + mechanical differentials leads to a moderate degradation of the manoeuvre time of 3–4.5%, with respect to the 4 WIM + 2 WS configuration.

To conclude the analysis it is worth pointing out that the implementation of the causal torque distribution strategy is only dependent on the values of the steering angle and vehicle acceleration, which are variables easily available on-board of everyday cars.

6. Concluding remarks and outlook

In this work, torque allocation strategies for EVs endowed with 4 WIMs have been studied, targeting the full exploitation of the performance benefits associated with this wheel drive system. To evaluate the causal controller, a minimum-time optimal problem was formulated, the solution of which provided a benchmark against which causal strategies can be objectively compared. Furthermore, a sub-optimal, causal, allocation strategy was designed, with the goal of maximising the performance envelope of the EV. Such a solution, which can be implemented online, allows exploiting the full vehicle capabilities, with a performance loss of less than 1% in manoeuvre time with respect to the benchmark solution, and it is transparent for the driver, thus maintaining the vehicle driveability. Future work will consider the joint

optimisation of performance and energy efficiency, addressing also fail safe operation in case possible actuator faults. Furthermore, we plan to further investigate the potential relationships between vehicle- and lap-time/performance. In this respect, we also aim to investigate how a racing driver rates the characteristics generated by the proposed allocation strategy, in order to assess the acceptance of the proposed performance-oriented policies.

Note

1. Assuming 50/50 weigh distribution in the left/right wheels.

References

[1] Chen Y, Wang J. Fast and global optimal energy-efficient control allocation with applications to over-actuated electric ground vehicles. IEEE Trans Control Syst Technol. 2012;20(5):1202–1211.

[2] de Castro R, Araujo RE, Oliveira H. Design, development and characterisation of a FPGA platform for multi-motor electric vehicle control. In: The 5th IEEE Vehicle Power and Propulsion Conference. Dearborn, USA; 2009.

[3] de Castro RP, Oliveira HS, Soares JR, Cerqueira NM, Araujo RE. A new FPGA based control system for electrical propulsion with electronic differential. In: Power Electronics and Applications, 2007 European Conference on. Aalborg, Denmark; 2007;1–10.

[4] Haddoun A, El Hachemi Benbouzid M, Diallo D, Abdessemed R, Ghouili J, Srairi K. Modeling, analysis, and neural network control of an EV electrical differential. Industrial Electronics, IEEE Trans. 2008;55(6):2286–2294.

[5] Tabbache B, Kheloui A, Benbouzid MEH. An adaptive electric differential for electric vehicles motion stabilization. IEEE Trans Veh Technol. 2011;60(1):104–110.

[6] Yan C, Junmin W. Design and evaluation on electric differentials for overactuated electric ground vehicles with four independent in-wheel motors. IEEE Trans Veh Technol. 2012;61(4):1534–1542.

[7] Rajamani R. Vehicle dynamics and control. New York: Springer; 2006.

[8] Canale M, Fagiano L, Milanese M, Borodani P. Robust vehicle yaw control using an active differential and IMC techniques. Control Eng Pract. 2007;15(8):923–941.

[9] He P, Hori Y, Kamachi M, Walters K, Yoshida H. Future motion control to be realized by in-wheel motored electric vehicle. In: Industrial Electronics Society, 2005. IECON 2005. 31st Annual Conference of IEEE; Raleigh, NC, USA; 2005.

[10] Deur J, Assadian F, Hancock M. Parameter optimization of PID class of yaw rate controllers. In: Proceedings of UKACC International Conference on CONTROL; Coventry, UK; 2010.

[11] Masaki N, Iwano H, Kamada T, Nagai M. Vehicle dynamics control of in-wheel electric motor drive vehicles based on averaging of tire force usage. J Mech Syst Transp Logist. 2012;5:14–29.

[12] Hancock MJ, Williams RA, Fina E, Best MC. Yaw motion control via active differentials. Trans Inst Meas Control. 2007;29(2):137–157.

[13] Esmailzadeh E, Goodarzi A, Vossoughi GR. Optimal yaw moment control law for improved vehicle handling. Mechatronics. 2003;13(7):659–675.

[14] Canale M, Fagiano L, Ferrara A, Vecchio C. Vehicle yaw control via second-order sliding-mode technique. IEEE Trans Ind Electron. 2008;55(11):3908–3916.

[15] Juyong K, Jinho Y, Kyongsu Y. Driving control algorithm for maneuverability, lateral stability, and rollover prevention of 4WD electric vehicles with independently driven front and rear wheels. IEEE Trans Veh Technol. 2011;60(7):2987–3001.

[16] Canale M, Fagiano L, Razza V. Approximate NMPC for vehicle stability: design, implementation and SIL testing. Control Eng Pract. 2010;18(6):630–639.

[17] Bianchi D, Borri A, Domenica Di Benedetto M, Di Gennaro S. Adaptive integrated vehicle control using active front steering and rear torque . Int J Veh Auton Syst. 2010;8(2/3/4):85–105.

[18] Jonasson M, Andreasson J. Exploiting autonomous corner modules to resolve force constraints in the tyre contact patch. Veh Syst Dyn. 2008;46(7):553–573.

[19] Jonasson M. Exploiting individual wheel actuators to enhance vehicle dynamics and safety in electric vehicles [Phd thesis]. KTH – Royal Institute of Technology; 2009.

[20] de Castro R, Tanelli M, Araújo RE, Savaresi SM. Torque allocation in evs with 4 in-wheel motors: a high-performance approach. In: 23nd International Symposium on Dynamics of Vehicles on Roads and Tracks. Qingdao, China; 2013;1–6.

[21] Sharp RS, Peng H. Vehicle dynamics applications of optimal control theory. Veh Syst Dyn. 2011;49(7):1073–1111.

[22] Kelly DP, Sharp RS. Time-optimal control of the race car: a numerical method to emulate the ideal driver. Veh Syst Dyn. 2010;48(12):1461–1474.
[23] Casanova D, Sharp RS, Symonds P. Minimum time manoeuvring: the significance of yaw inertia. Veh Syst Dyn. 2000;34(2):77–115.
[24] Klomp M. Longitudinal force distribution using quadratically constrained linear programming. Veh Syst Dyn. 2011;49(12):1823–1836.
[25] Peng H, Hu J-S. Traction/braking force distribution for optimal longitudinal motion during curve following. Veh Syst Dyn. 1996;26(4):301–320.
[26] Sawase K, Ushiroda Y. Improvement of vehicle dynamics by right-and-left torque system in various drivetrains. Mitsubishi Motors – Tech Rev. 2008;20:18–24.
[27] Wang JM, Longoria RG. Coordinated and reconfigurable vehicle dynamics control. IEEE Trans Control Syst Technol. 2009;17(3):723–732.
[28] Geng C, Mostefai L, Denai M, Hori Y. Direct yaw-moment control of an in-wheel-motored electric vehicle based on body slip angle fuzzy observer. IEEE Trans Ind Electron. 2009;56(5):1411–1419.
[29] Kiencke U, Nielsen L. Automotive control systems for engine, driveline, and vehicle. 2nd ed. Berlin: Springer-Verlag; 2005.
[30] Pacejka HB. Tyre and vehicle dynamics. Oxford (UK): Butterworth-Heinemann; 2002.
[31] Gerdts M, Karrenberg S, Bebler BM, Stock G. Generating locally optimal trajectories for an automatically driven car. Optim Eng. 2009;10(4):439–463.
[32] Rao AV. A survey of numerical methods for optimal control. In: AAS/AIAA Astrodynamics Specialist Conference. Savannah, Georgia, USA; 2009.
[33] Betts JT. Practical methods for optimal control and estimation using nonlinear programming. Soc Ind Appl Math. 2010. doi:10.1137/1.9780898718577
[34] Wachter A, Biegler LT. On the implementation of a primal-dual interior point filter line search algorithm for large-scale nonlinear programming. Math Program. 2006;106(1):25–57.
[35] Sharp RS, Casanova D, Symonds P. A mathematical model for driver steering control, with design, tuning and performance results. Veh Syst Dyn. 2000;33(5):289–326.
[36] Genta G, Morello L. The automotive chassis, volume 2: system design. Berlin: Springer; 2009.
[37] Milliken WF, Milliken DL. Race car vehicle dynamics. Warrendale, PA: SAE International; 1995.

Appendix 1. Model parameters

See Table A1.

Table A1. Parameters of the employed vehicle model.

Variable	Symbol	Value
Vehicle mass	m	1100 kg
Yaw inertia	I_z	1800 kg m^2
Distance between front axle and COG	a	1.2 m
Distance between rear axle and COG	b	1.3 m
COG height	h	0.54 m
Trackwidth	c	1.6 m
Coefficient of rolling resistance	f_r	0.013
Aero. drag coefficient (frontal)	C_x	0.35
Aero. drag coefficient (lateral)	C_y	3
Frontal area	A_x	1.8 m
Lateral area	A_y	2.7 m
Air density	ρ	1.206 kg/m^3
Wheel radius	r	0.3 (m)
MTF parameter B	B	7
MTF parameter C	C	1.6
MTF parameter D	D	1
Maximum front steer	$\bar{\delta}_F$	35°

Appendix 2. Definition of the disturbance

The model (1) is also disturbed by the vector $\Delta = [\Delta_x \ \ \Delta_y \ \ \Delta_\psi]^T$, associated with the aerodynamic drag and rolling resistance forces,[29]

$$\Delta_x = f_r mg + \nu_x v_x^2, \quad \Delta_y = \nu_y |v_y| v_y, \quad \Delta_\psi = 0, \tag{A1a}$$

where f_r is the rolling resistance coefficient, and $\nu_k = (\rho/2) C_k A_k$, $k \in \{x, y\}$, the aero coefficients (see Table A1 for the parameters' definition). For simplicity, the grade forces were neglected, since only planar motion is being considered, and positive longitudinal speeds were assumed (i.e. $v_x > 0$).